CRYSTAL GROWTH & DESIGN

pubs.acs.org/crystal

Article

Field-Induced Slow Relaxation of the Magnetization in Two Families of [$M^{II}Ln^{III}$] Complexes

Ernesto Costa-Villén, Mercè Font-Bardia, Júlia Mayans, and Albert Escuer*

Cite This: *Cryst. Growth Des.* 2024, 24, 5806−5817

Read Online

ACCESS | Metrics & More | Article Recommendations | Supporting Information

ABSTRACT: A family of discrete dinuclear complexes [$M^{II}Ln^{III}$] (M = Cu, Ni and Ln = Ce, Gd, Tb, Dy, Er, Yb) has been synthesized from the use of the compartmental Schiff base ligand H_4L (3,3′-((1*E*,1′*E*)-(ethane-1,2-diylbis-(azaneylylidene)) bis(methaneylylidene))bis(benzene-1,2-diol)), obtained from the condensation of ethylenediamine and 2,3-dihydroxybenzaldehyde. All of the complexes have been structurally and magnetically characterized. The dynamic magnetic measurements show that the [$Cu^{II}Ln^{III}$] and [$Ni^{II}Ln^{III}$] derivatives exhibit ac response as a function of the d-cation. Noteworthily, the isotropic Gd^{III} complexes exhibit a slow relaxation of magnetization.

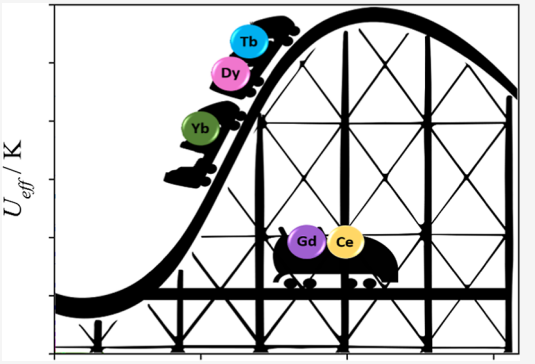

INTRODUCTION

Coordination chemistry using Schiff bases, the N-analogues of carbonyl functional groups (aldehydes and ketones), where the C═O bond is replaced by one C═N bond, is today an extremely large research field. Schiff bases have been widely used as organic ligands in coordination chemistry over many years for synthesizing compounds for different purposes related to biological activity,[1−3] catalysis,[4,5] chemical sensing,[6,7] luminescence,[8,9] magnetism,[10,11] and antioxidant or antimicrobial activity.[12,13] This wide variety in possible applications is because the number of available Schiff bases for synthesis is almost infinite due to the large amount of possible precursors of the condensation between the amino and the carbonyl groups. A careful selection of these precursors allows control over the denticity of the ligand, the charge of the deprotonated ligand, the nature of the donor atoms, and/or the nature of the chelating moieties, giving a platform to design specific ligands for each purpose.

Compartmental Schiff bases are a particular case in which two well-differentiated cavities of different sizes and/or donor atoms are able to link different types of cations, favoring heterometallic complexes. This kind of complexes are usually synthesized from the condensation of one equivalent of a diamine with two equivalents of a carbonyl group, either aldehydes or ketones, to generate the compartmental ligands, where the smaller compartment usually hosts a first−row transition cation while the larger compartment can host a second 3d cation or a larger cation such as lanthanides.

Pyridylaldehyde or salicylaldehyde as carbonyl condensing groups are adequate to build tetradentate Schiff bases whereas the most used aldehyde has been *o*-vanillin which is useful to design compartmental hexadentate ligands, being magnetic, catalytic, and luminescent studies the most common by far.[11,14−16]

Focusing on the magnetic properties, despite the large number of works reporting static susceptibility measurements, there are few studies on their dynamic properties, and it becomes surprising that very similar compounds present different slow relaxation of the magnetization (SRM) response. We have been working in this topology of compounds over the last years,[17−23] and we continue seeing despairing behaviors on the magnetic properties. For this reason, to provide new data on the slow relaxation of the magnetization of this family of compounds, we synthesized two new series of compounds employing the H_4L ligand obtained from the condensation of ethylenediamine and 2,3-dihydroxybenzaldehyde (Chart 1, left). This hexadentate ligand incorporates two extra −OH

Chart 1. Structural Formula and Coordination Mode of the H_4L Ligand Employed in This Work

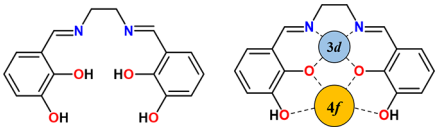

Received: April 30, 2024
Revised: June 11, 2024
Accepted: June 11, 2024
Published: June 25, 2024

groups and a larger potential negative charge after deprotonation. This ligand and the related ones derived from 2-methyl-1,2-propanediamine, 2,2′-dimethyl-1,2-butanediamine or 1,2-cyclohexanediamine have been actively employed in actinides chemistry with cations such as U^{IV}[24−33] and Th^{IV}[33,34] but it has been practically unexplored in the characterization of bicompartmental 3d−4f Schiff base-derived compounds, with only two heterometallic {CuLnCu} Ln = Gd^{III}, Tb^{III} reported examples.[35]

The target of the present work has been to prepare heterometallic 3d−4f systems employing the paramagnetic $S = 1/2$ Cu^{II} ion or the diamagnetic square planar Ni^{II} cation combined with different lanthanides with the formula $[CuCe(H_2L)(NO_3)_3(MeOH)]\cdot MeOH$ (**1CuCe·MeOH**), $[CuLn(H_2L)(NO_3)_3]\cdot 2MeOH$ Ln = Gd^{III} (**2CuGd·2MeOH**), Tb^{III} (**3CuTb·2MeOH**), Dy^{III} (**4CuDy·2MeOH**), Er^{III} (**5CuEr·2MeOH**) and Yb^{III} $[CuYb(H_2L)(NO_3)_3(MeOH)]\cdot 2MeOH$ (**6CuYb·2MeOH**), $[NiLn(H_2L)(NO_3)_3]\cdot 4MeOH$ [Ln = Ce^{III} (**7NiCe·4MeOH**), Gd^{III} (**8NiGd·4MeOH**), Tb^{III} (**9NiTb·4MeOH**), Dy^{III} (**10NiDy·4MeOH**), Er^{III} (**11NiEr·4MeOH**)], and $[Ni_2Yb(H_2L)(HL)][NiYb(H_2L)(NO_3)_3](NO_3)_3](NO_3)_2\cdot 3MeOH\cdot Et_2O$ (**12NiYb·3MeOH·Et$_2$O**) in which the 3d cations are always placed in the inner cavity of the ligand and the 4f cations occupy the outer O-rich cavity (Chart 1, right).

The exploration of their magnetic properties and the comparison with previously reported related systems show clear differences in their SRM as a function of the d-cation. The two complexes **2CuGd** and **8NiGd** provided new examples of the unusual out-of-phase response of the isotropic Gd^{III} cation.

EXPERIMENTAL SECTION

X-ray Crystallography. Powder X-ray diffraction was performed with a PANalytical X'Pert PRO MPD q/q powder diffractometer of 240 mm radius, in a configuration of convergent beam with a focalizing mirror and a transmission geometry with flat samples sandwiched between low absorbing films and CuKa radiation (l = 1.5418 Å). Powder spectra for the {CuLn} series evidence isostructurality between **2CuGd**, **3CuTb**, and **4CuDy** (Figure S1). Cell determination shows isostructurality for the complete {NiLn} series with the exception of the **12NiYb** complex (Table S1).

To have a complete structural characterization, orange (**1CuCe**, **2CuGd**, **6CuYb**, **7NiCe**, **8NiGd**, **11NiEr**, and **12NiYb**) prism-like specimens were used for the X-ray crystallographic analysis. The X-ray intensity data was measured on a D8 Venture system equipped with a multilayer monochromator and a Mo microfocus. The frames were integrated with the Bruker SAINT software package by using a narrow-frame algorithm. The structures were solved and refined using the Bruker SHELXLE Software.[36]

Crystal data and refinement details for complexes **1CuCe**, **2CuGd**, **6CuYb**, **7NiCe**, **8NiGd**, **11NiEr**, and **12NiYb** are summarized in Tables S2 and S3. Further crystallographic details can be found in the corresponding CIF files provided in the Supporting Information.

Materials and Methods. All measurements were performed on crushed well-formed crystals of the corresponding complex. Magnetic susceptibility measurements were carried out on pressed polycrystalline samples with an MPMS5 Quantum Design susceptometer working in the range of 30−300 K under magnetic fields of 0.3 T and under a field of 0.03 T in the 30−2 K range to avoid saturation effects at low temperature. Diamagnetic corrections were estimated from Pascal Tables.[37] Infrared spectra (4000−400 cm^{-1}) were recorded from KBr pellets on a Bruker IFS-125 FT-IR spectrophotometer.

Synthesis. Ethylenediamine, 2,3-dihydroxybenzaldehyde, Cu^{II}, Ni^{II}, and Ln^{III} nitrates, and reagent-grade solvents were used as they were purchased. The synthesis of the reported complexes was performed in the absence of a base. Trials to promote a larger deprotonation of the ligand in a basic medium led to the immediate precipitation of compounds as powder which were insoluble in the common solvents.

Synthesis of the H_4L Ligand. The synthesis of the ligand was accomplished following a modification of the reported method[38] by reaction of ethylenediamine (0.106 g, 1.6 mmol) with 2,3-dihydroxybenzaldehyde (0.459 g, 3.33 mmol) in 20 mL of MeOH. Each reagent was dissolved in 10 mL of MeOH and both solutions were mixed and kept with continuous stirring for 20 min. The orange precipitate was filtered to obtain 3,3′-((1*E*,1′*E*)-(ethane-1,2-diylbis(azaneylylidene)) bis(methane-ylylidene)) bis(benzene-1,2-diol) (**H_4L**) as an orange powder with a yield of 80%.

$[CuCe(H_2L)(NO_3)_3(MeOH)]\cdot MeOH$ (1CuCe·MeOH), $[CuLn(H_2L)(NO_3)_3]\cdot 2MeOH$ Ln = Gd^{III} (2CuGd·2MeOH), Tb^{III} (3CuTb·2MeOH), Dy^{III} (4CuDy·2MeOH), Er^{III} (5CuEr·2MeOH), and Yb^{III} $[CuYb(H_2L)(NO_3)_3(MeOH)]\cdot 2MeOH$ (6CuYb·2MeOH). H_4L (0.075 g, 0.25 mmol) and $Cu(NO_3)_2\cdot 3H_2O$ (0.060 g, 0.25 mmol) were dissolved in MeOH (15 mL). The mixture turned brown, and a precipitate appeared. The mixture was kept under continuous stirring for 10 min at room temperature and 0.25 mmol the corresponding lanthanide salt ($Ce(NO_3)_3\cdot 6H_2O$ (0.109 g), $Gd(NO_3)_3\cdot 6H_2O$ (0.113 g), $Tb(NO_3)_3\cdot 6H_2O$ (0.113 g), $Dy(NO_3)_3\cdot 6H_2O$ (0.114 g), $Er(NO_3)_3\cdot 6H_2O$ (0.115 g) or $Yb(NO_3)_3\cdot 5H_2O$ (0.112 g)) was added to the mixture to give a clear reddish-brown solution. The resulting solutions were kept under stirring for a further 10 min, filtered, and slowly diffused with diethylether. $[CeCu(H_2L)(NO_3)_3MeOH]\cdot MeOH$ (**1CuCe**) $[CuGd(H_2L)(NO_3)_3]\cdot 2MeOH$ (**2CuGd**), $[CuTb(H_2L)(NO_3)_3]\cdot 2MeOH$ (**3CuDy**), $[CuDy(H_2L)(NO_3)_3]\cdot 2MeOH$ (**4CuTb**), $[CuEr(H_2L)(NO_3)_3]\cdot 2MeOH$ (**5CuEr**), and $[CuYb(H_2L1)(NO_3)_3MeOH]\cdot 2MeOH$ (**6CuYb**) were obtained as reddish-brown prism-like crystals suitable for X-ray diffraction in a period of 2 days. Analytical data are summarized in Table S4 and IR spectra are reported in Figures S2−S4.

$[NiLn(H_2L)(NO_3)_3]\cdot 4MeOH$, Ln^{III} = Ce^{III} (7NiCe·4MeOH), Gd^{III} (8NiGd·4MeOH), Tb^{III} (9NiTb·4MeOH), Dy^{III} (10NiDy·4MeOH), and Er^{III} (11NiEr·4MeOH). The complexes were prepared following the same procedure employed for **1**−**6**: H_4L (0.075 g, 0.25 mmol) and $Ni(NO_3)_2\cdot 6H_2O$ (0.072 g, 0.25 mmol) were mixed and dissolved in MeOH (15 mL). The mixture turned brown, a precipitate appeared, and the mixture was maintained under continuous stirring for 10 min at room temperature. Addition of 0.25 mmol of the corresponding nitrate ($Ce(NO_3)_3\cdot 6H_2O$ (0.109 g), $Gd(NO_3)_3\cdot 6H_2O$ (0.113 g), $Tb(NO_3)_3\cdot 6H_2O$ (0.113 g), $Dy(NO_3)_3\cdot 6H_2O$ (0.114 g), $Er(NO_3)_3\cdot 6H_2O$ (0.115 g)) gave a clear reddish-brown solution and stirred for 10 additional minutes and slowly diffused with diethylether. $[CeNi(H_2L)(NO_3)_3]\cdot 4MeOH$ (**7NiCe**), $[GdNi(H_2L)(NO_3)_3]\cdot 4MeOH$ (**8NiGd**), $[NiTb(H_2L)(NO_3)_3]\cdot 4MeOH$ (**9NiTb**), $[DyNi(H_2L)(NO_3)_3]\cdot 4MeOH$ (**10NiDy**), and $[ErNi(H_2L)(NO_3)_3]\cdot 4MeOH$ (**11NiEr**) were obtained as reddish-brown prism-like crystals in a few days. Analytical data are summarized in Table S4 and IR spectra are reported in Figures S5 and S6.

$[Ni_2Yb(H_2L)(HL)][NiYb(H_2L)(NO_3)_3](NO_3)_2\cdot 3MeOH\cdot Et_2O$ (12NiYb). Following the procedure described above, and $Yb(NO_3)_3$ (0.112 g, 0.25 mmol) the title complex with formula $[Ni_2Yb(H_2L)(H_1L)][NiYb(H_2L)(NO_3)_3](NO_3)_2\cdot 3MeOH\cdot Et_2O$ (**12NiYb**) was obtained despite its $3Ni^{II}$:$2Ln^{III}$ ratio as reddish-brown prismatic crystals. Analytical data are summarized in Table S4 and IR spectra are reported in Figure S7.

RESULTS AND DISCUSSION

Description of the Structures. The structures of the reported complexes exhibit some common features, and thus, to avoid repetitive descriptions, the structures of **1CuCe**, **7NiCe**, and **12NiYb** will be described in detail and only the most remarkable differences will be explained for the remaining complexes of each series.

https://doi.org/10.1021/acs.cgd.4c00598
Cryst. Growth Des. 2024, 24, 5806−5817

[CuCe(H$_2$L)(NO$_3$)$_3$(MeOH)]·MeOH (1CuCe·MeOH). A partially labeled plot of **1CuCe** is shown in Figure 1, top.

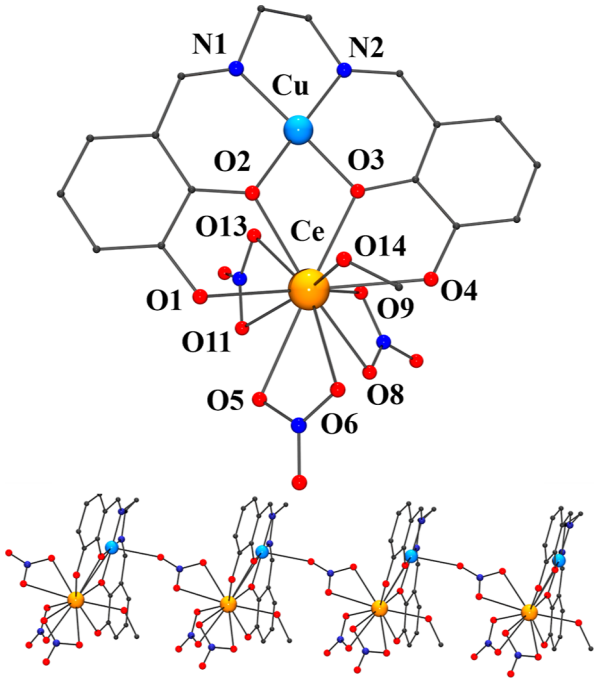

Figure 1. Top, partially labeled plot of **1CuCe**. Hydrogens were removed for the sake of clarity. Bottom, visualization of compound **1CuCe** along the (0 0 1) vector. Color code: Cu^{II} cyan, Ce^{III} orange, O red, N navy, and C gray.

Selected bond parameters and angles are summarized in Table S5. The molecular structure of **1CuCe** consists of a neutral dinuclear complex of Cu^{II} and Ce^{III} that crystallizes in the $P\bar{1}$ triclinic system. The Cu^{II} cation is located in the inner N_2O_2 cavity of the ligand while the Ce^{III} cation is placed in the external O_4 cavity. The inner hydroxo functional groups of the Schiff base are deprotonated and act as bridges between the Cu^{II} and Ce^{III} cations whereas the external hydroxo functions remain protonated, resulting in the H$_2$L^{2-} ligand. In addition to the four O-donors from the Schiff base, the Ce^{III} cation is bonded to three bidentate nitrato ligands and one methanol molecule, resulting in an undecacoordinated environment.

The environment around the Ce^{III} cation is formed for three short bond distances to the deprotonated O2 and O3 donors (2.531(5)−2.469(4) Å) and to the coordinated methanol (Ce−O14, 2.535(5) Å), and larger bond distances to the protonated O1 and O4 atoms (2.625(5)−2.692(4) Å) from the H$_2$L^{2-} ligand and six O-donors from the bidentate nitrato ligands in the 2.604(5)−2.724(5) Å range. The O2−Ce−O3 bond angle is 61.1(1)°, and the O−Ce−O bond angles involving the bidentate nitrates are comprised in the range of 47.7(1)−48.1(1)°. The Ce-(O)$_2$−Cu fragment is not planar, defining a dihedral angle between the Ce−O2−O3 and Cu−O2−O3 mean planes of 14.5(2)°.

One of the nitrato ligands bonded to the Ce^{III} cations also links to the axial coordination site of one Cu^{II} cation from the neighboring dimer resulting in a pentacoordinated square pyramidal N_2O_3 environment and a 1D arrangement of dimers along the *a*-axis of the network, Figure 1, bottom. The Cu−N and Cu−O distances involving the H$_2$L^{2-} organic ligand are similar, ranging between 1.902(5) and 1.931(5) Å, and the axial Cu−O12 distance to the O-donor from the nitrato bridge is 2.540(6) Å. The O2−Cu−O3 [83.9(2)°] and N1−Cu−N2 [86.0(2)°] bond angles are shorter than the N−Cu−O bond angles [94.8(2)° and 95.2(2)°].

SHAPE[39] calculations have been performed for the Ce^{III} cation, indicating a very distorted environment with respect to any polyhedron, being a capped pentagonal antiprism the closest one with a very large CShM value of 3.692 (Table S6 and Figure S8). Such a degree of distortion, due to the low bite of the double hydroxo bridge and the nitrato ligands, excludes a polyhedron assignation, and its environment should be defined as C_1 symmetry.

[CuGd(H$_2$L)(NO$_3$)$_3$]·2MeOH (2CuGd) and [CuYb(H$_2$L)(NO$_3$)$_3$MeOH]·2MeOH (6CuYb). The molecular structure of neutral dinuclear complexes **2CuGd** and **6CuYb** is similar, in general trends, to complex **1CuCe** with differences derived from the progressive reduction of the ionic radii for heavier lanthanoid cations. A partially labeled plot of **2CuGd** and **6CuYb** are shown in Figure 2. Selected bond parameters and angles for **2CuGd** and **6CuYb** are summarized in Tables S7 and S8.

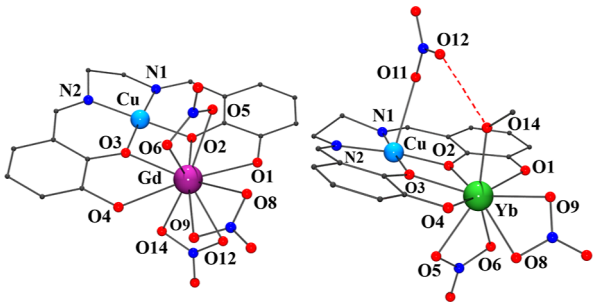

Figure 2. Partially labeled plot of **2CuGd** (left) and **6CuYb** (right). Hydrogens have been removed and only heteroatoms are labeled for the sake of clarity. Red dashed lines show the intramolecular H-bond between the coordinated nitrato and methanol ligands. Color code: Cu^{II} cyan, Gd^{III} purple, Yb^{III} green, O red, N navy, and C gray.

As in the previous case, the ligand is bisdeprotonated (H$_2$L^{2-}), and the Cu^{II} and Ln^{III} cations are located respectively in the inner and outer cavities of the compartmental H$_2$L^{2-} ligand. The main differences lie in the coordination environments of both cations. For **2CuGd**, the Gd^{III} links the four O-donors from the H$_2$L^{2-} ligand and three bidentate nitrato ligands, resulting in a decacoordinated environment. In this case, the nitrato ligands do not link the axial sites of the Cu^{II} cation which remains in a N_2O_2 square planar environment. For **6CuYb**, the Yb^{III} cation is bonded to the four O-donors from the H$_2$L^{2-} ligand, two bidentate nitrato ligands, and one methanol molecule, resulting in an enneacoordinated environment. The third nitrato that fulfills the charge balance of the molecule acts as a monodentate ligand, linked to the axial coordination site of the Cu^{II} cation which adopts an N_2O_3 square pyramidal environment. An intramolecular H-bond between the O12-atom of the nitrate coordinated to the Cu^{II} cation and the methanol molecule linked to the Yb^{III} cation [O12...O14 distance of 2.732(2) Å] helps to stabilize the neutral molecule.

SHAPE[39] calculations also indicate that the closer coordination polyhedron around the Ln^{III} cations is an ideal tetradecahedron with a moderate deviation of CShM = 1.84 for **2CuGd** (Table S9 and Figure S8), and muffin geometry with a

https://doi.org/10.1021/acs.cgd.4c00598
Cryst. Growth Des. 2024, 24, 5806−5817

deviation of CShM = 2.51 (Table S10 and Figure S8) for **6CuYb**, strongly influenced by the small bite of the bidentate ligands.

The reduction of the radii of the lanthanoid cation along the series has a consequence of the reduction of the Ln−O bond distances, the Ln...Cu distance, the coordination number, and an increase of the planarity of the core, Table 1.

Table 1. Comparative Values for the Main Bond Parameters (Å) and Coordination Number (C.N.) Related with the Ln^{III} Cation for 1CuCe, 2CuGd, and 6CuYb

	1CuCe	2CuGd	6CuYb
Ln^{III} C.N.	11	10	9
Ln−O2	2.531(5)	2.392(1)	2.276(2)
Ln−O3	2.469(5)	2.3882(9)	2.279(2)
O2−Ln−O3	61.1(1)	63.01(3)	64.61(5)
O2−Cu−O3	83.9(2)	82.33(4)	80.22(7)
Cu−O2−Ln	105.1(2)	107.09(4)	107.45(6)
Cu−O3−Ln	107.4(2)	107.23(4)	107.70(7)
Cu...Ln	3.5390(9)	3.4628(3)	3.3696(3)
Ln−O2−O3−Cu	14.5(2)	5.45(5)	1.53(8)

*$[LnNi(H_2L)(NO_3)_3]\cdot 4MeOH$ Ln = Ce, (**7NiCe**), Ln = Gd (**8NiGd**) and Ln = Er (**11NiEr**).* A partially labeled plot of the isostructural NiLn complexes **7NiCe**, **8NiGd**, and **11NiEr** is shown in Figure 3. Selected bond parameters and angles are

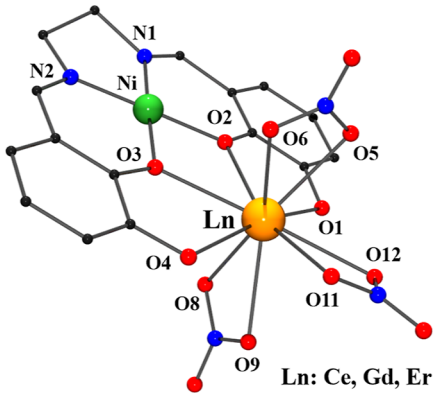

Figure 3. Partially labeled plot of the molecular structure of the **7NiCe**, **8NiGd**, and **11NiEr**. Hydrogens have been removed and only heteroatoms are labeled for the sake of clarity. Color key Ni^{II} forest green, $Ce^{III}/Gd^{III}/Er^{III}$ orange, O red, navy, and C gray.

summarized in Table S11. The structure of the three complexes consists of a neutral dinuclear complex of Ni^{II} and Ln^{III}, with the Ni^{II} cation located in the inner cavity of the ligand while the Ln^{III} cation is placed in the outer oxygenated cavity.

The cations are linked to one doubly deprotonated hexadentate H_2L^{2-} ligand and three bidentate nitrato ligands bonded to the Ln^{III} atom, resulting in a decacoordinated environment for the lanthanoid in the three complexes. The two N−donor atoms and two O−donor atoms from the organic ligand H_2L^{2-} are coordinated to the Ni^{II} cation with similar and short Ni−N and Ni−O bond distances ranging between 1.848(3) and 1.860(2) Å, typical of a square-planar environment in contrast with the previously described {CuLn} complexes. The Ln−O distances are similar for the O-phenoxo bridge, the protonated phenolic ligand, or the O-nitrate donors in the short-range 2.494(2)−2.610(3) Å for **7NiCe**, 2.420(3)−2.499(4) Å for **8NiGd**, and 2.341(3)−2.578(4) for **11NiEr**. SHAPE[39] calculations have been performed for the Ln^{III} cations indicating an arrangement close to a tetradecahedron (Table S12 and Figure S9) with a moderate deviation of CShM = 1.50 (Ce^{III}), 1.68 (Gd^{III}), and 2.66 (Er^{III}) from the ideal polyhedron.

$[Ni_2Yb(H_2L)(HL)][NiYb(H_2L)(NO_3)_3](NO_3)_2\cdot 3MeOH\cdot Et_2O$ (12NiYb). Complex **12NiYb** consists of one neutral {NiYb} dinuclear unit, one dianionic {NiYbNi} trinuclear complex, two ionic nitrate anions, and solvent molecules. A partially labeled plot of the two components of **12NiYb** is shown in Figure 4. Selected bond parameters and angles are summarized

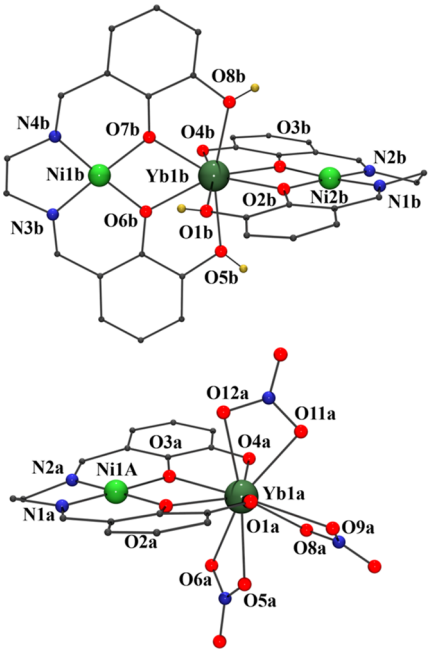

Figure 4. Top, partially labeled plot of the cationic trimeric unit of complex **12NiYb** showing the three protonated hydroxo functions. Bottom, partially labeled plot of the neutral dimeric unit of complex **12NiYb**. Color key Ni^{II} forest green, Yb^{III} dark green, O red, N navy, and C gray.

in Table S13. The dinuclear unit is similar to the previously described Ce^{III} or Gd^{III} complexes, maintaining the same level of deprotonation for the ligand (H_2L^{2-}), the square planar coordination for the Ni^{II} cation and the decacoordinated environment for the Yb^{III} formed by the four O-donors from the Schiff base and three bidentate nitrato ligands.

In contrast with the copper analogous described above, the coordination number remains constant along the complete series from Ce^{III} to Yb^{III} and the changes derived from the decrease in the ionic radii along the series are limited to the bond parameters directly related with the lanthanoids (Table 2).

The cationic trinuclear unit is formed by one neutral $[NiH_2L]$ and one anionic $[NiHL]^-$ fragments that act as complex as a ligand coordinating one Yb^{III} cation by means of the eight O-donors from the two Schiff bases. The charge balance is fulfilled with two ionic nitrates. The Ni^{II} cations are placed in the corresponding N_2O_2 inner cavities of the ligands in a square planar environment with short Ni−N and Ni−O bond distances comprised between 1.810(3) and 1.842(2) Å.

https://doi.org/10.1021/acs.cgd.4c00598
Cryst. Growth Des. 2024, 24, 5806−5817

Table 2. Comparative Values for the Bond Parameters (Å) and Coordination Number (C.N.) Related with the Ln^{III} Cation for 7NiCe, 8NIGd, 11NiEr, and the Dinuclear Unit of 12NiYb

	7NiCe	8NiGd	11NiEr	12NiYb
Ln^{III} C.N.	10	10	10	10
Ln−O2	2.494(2)	2.444(3)	2.341(3)	2.315(2)
Ln−O3	2.509(2)	2.420(3)	2.413(3)	2.340(2)
O2−Ln−O3	58.42(7)	59.3(1)	60.2(1)	61.31(7)
O2−Ni−O3	82.32(9)	81.2(2)	80.7(1)	80.42(9)
Ni−O2−Ln	109.54(8)	109.3(2)	110.1(1)	109.32(9)
Ni−O3−Ln	109.31(8)	109.8(2)	107.5(1)	108.54(9)
Ni...Ln	3.5754(9)	3.5117(9)	3.4450(9)	3.4017(9)
Ln−O2−O3−Ni	5.8(1)	6.1(2)	10.9(2)	5.9(1)

Noteworthy, one of the Schiff bases is similar to the previously described complexes with the deprotonated bridging hydroxo groups (H_2L^{2-}), whereas the second base exhibits one additional deprotonated hydroxo group (HL^{3-}). The $[NiH_2L]$ and $[NiHL]^-$ fragments are roughly perpendicular with a dihedral angle between the mean NiN_2O_2 planes of 77.0°. The coordination environment around the Yb^{III} cation is formed by the eight O donors, showing different Yb−O bond distances: Yb−O bond distances to the bridging phenolate O-donors lie in the 2.270(2)−2.329(2) Å range, the distances to the protonated hydroxo groups are larger, ranging between 2.367(3)−2.418(2) Å and a short distance to the deprotonated phenoxo donor of 2.198(2) Å. The Yb−O−O−Ni fragments are essentially planar [torsions of 0.1(1)° and 2.8(1)°]. SHAPE calculations for the octacoordinated Yb^{III} cation suggest a triangular dodecahedron geometry (Table S14 and Figure S10) with a strong deviation of CShM = 3.41 from the ideal polyhedron due to the low bite of all the bidentate fragments that yields O−Yb−O bond angles lower than 65°.

The arrangement of the di and trinuclear units in the network consists of an alternated bidimensional arrangement of two layers of dimers and two layers of trimers, strongly interconnected by a set of H-bonds involving the crystallization methanol molecules, the nitrate counterions, and the protonated phenoxo groups from the Schiff bases, Figure S11.

Magnetic Properties. Static Measurements. DC magnetic susceptibility ($\chi_M T$) data for **1CuCe**, **2CuGd**, **3CuTb**, **4CuDy**, **5CuEr**, **6CuYb**, and **7NiCe**, **8NiGd**, **9NiTb**, **10NiDy**, **11NiEr**, **12NiYb** were measured on polycrystalline samples in the 2−300 K temperature range and plotted as $\chi_M T$ vs T (Figure 5, bottom). The isotropic **2CuGd** complex shows a room temperature $\chi_M T$ value of 9.00 $cm^3\ mol^{-1}\ K$, slightly larger than the theoretical value of 8.250 $cm^3\ mol^{-1}\ K$ ($g = 2.00$). On cooling the $\chi_M T$ value increases up to 10.79 $cm^3\ mol^{-1}\ K$ at 7.5 K suggesting a weak ferromagnetic intramolecular interaction. The magnetization measurement yields an M value of 8.43 $N_{\mu\beta}$ under the maximum field of 7 T in agreement with the expected value for one Gd^{III} cation and one Cu^{II} cation. The simultaneous fit of the susceptibility and magnetization data was performed with PHI software[40] using the spin-only Hamiltonian

$$H = -2J(S_{Cu} \times S_{Gd}) \quad (1)$$

resulting in the best−fit parameters of $J = +3.60(3)\ cm^{-1}$ and a global g value of 2.090(1). This response agrees either in sign and magnitude with the usual values for the interaction between Cu^{II} and Gd^{III}.[41−44]

At 300K, $\chi_M T$ for **1CuCe**, **3CuTb**, **4CuDy**, **5CuEr**, and **6CuYb** are 1.15, 13.22, 15.13, 11.78 and 2.99 $cm^3\ mol^{-1}\ K$, respectively, in good correlation with the theoretical values for the corresponding Ln^{III} plus one Cu^{II} noninteracting ions (1.175, 12.195, 14.545, 11.855 and 2.945 $cm^3\ mol^{-1}\ K$ respectively for $g = 2.00$) (Figure 5, top). When the temperature is lowered, $\chi_M T$ slightly decreases for **1CuCe**, **3CuTb**, **4CuDy**, **5CuEr**, and **6CuYb** down to 0.33, 11.75,

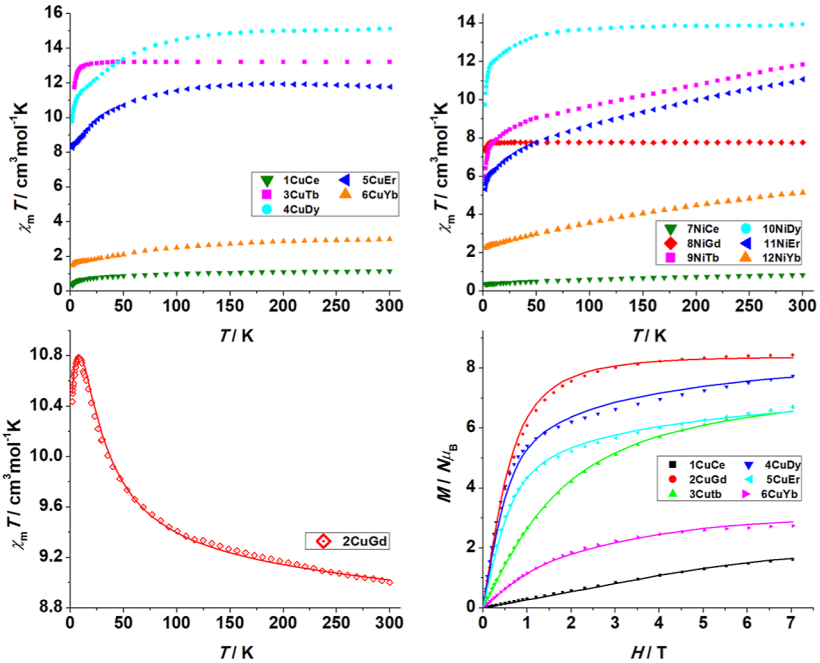

Figure 5. Top, $\chi_M T$ vs temperature plots for the families of complexes [**CuLn**] and [**NiLn**]. Bottom, $\chi_M T$ vs T for the isotropic 2CuGd complex (left) and magnetization plots for the [**CuLn**] series. Solid lines show the best fit of the data.

https://doi.org/10.1021/acs.cgd.4c00598
Cryst. Growth Des. 2024, 24, 5806−5817

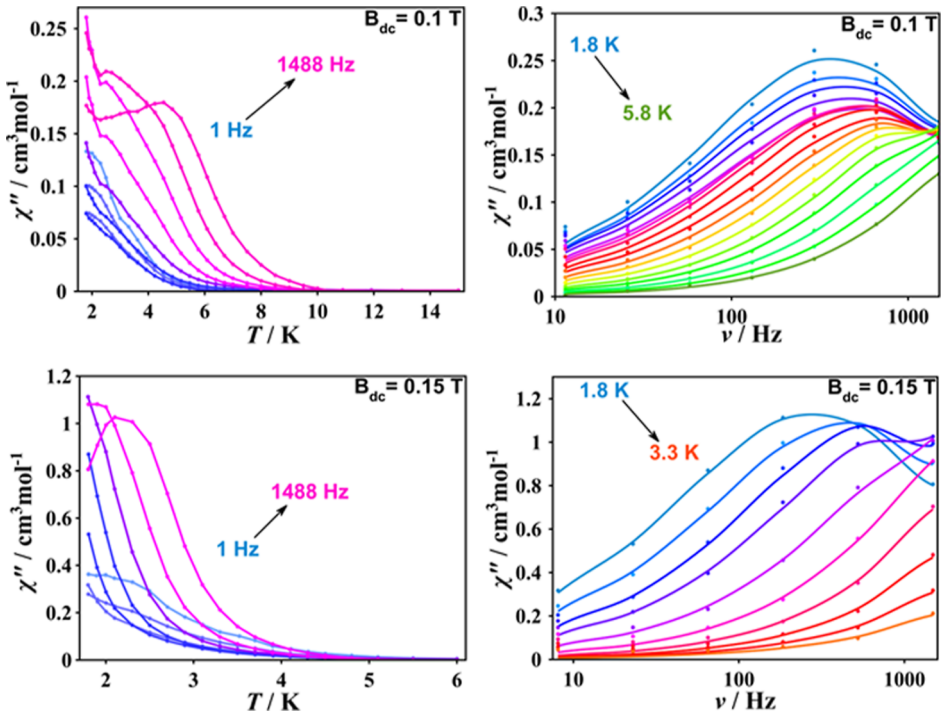

Figure 6. Temperature (left) and frequency (right) dependence of χ'' for complexes **2CuCe** (top) and **3CuTb** (bottom) at each optimal magnetic field.

9.78, 8.25, and 1.49 $cm^3\ mol^{-1}\ K$ at 2 K, respectively. The decrease in the susceptibility is due to the depopulation of the Stark levels modulated at low temperatures by weak intramolecular interactions. The magnetization measurements show maximum values that strongly deviate from the expected values and shape for noninteracting Ln^{III}–Cu^{II} pairs, reaching the values of 1.62, 6.71, 7.73, 6.69, and 2.73 $N_{\mu\beta}$ for **1CuCe**, **3CuTb**, **4CuDy**, **5CuEr**, and **6CuYb**, respectively (Figure 5, bottom).

For these complexes in which the lanthanoid possesses an orbital momentum $L \neq 0$, the susceptibility data were fitted with the PHI program[40] applying the anisotropic spin Hamiltonian

$$H = -2J(S_{Cu} \times S) + \lambda LS + D[L_z^2 - L(L+1)/3] + bH(-kL + 2S) \quad (2)$$

where S_{Cu} and S are the spin operators of the Cu^{II} and Ln^{III} cations, respectively, J coupling constant describes the strength of the Cu^{II}–Ln^{III} interaction, λ is the spin–orbit coupling parameter, Δ represents the axial zero-field splitting parameter of the Ln^{III} cation, and κ is the orbital reduction parameter, which is related with the grade of covalence (1.0 for fully ionic compounds). The fit was performed on the magnetization data, which are extremely sensitive to J and Δ and overcome the intramolecular interactions. Best fit values, fixing a g value of 2.10 for the Cu^{II} cation on the basis of the results for **2CuGd**, were $J = 5.57(5)\ cm^{-1}$, and $\Delta = -35.6(9)\ cm^{-1}$ for **1CuCe**, $J = 0.55(4)\ cm^{-1}$ and $\Delta = 26.2(4)\ cm^{-1}$ for **3CuTb**, $J = 0.9(1)\ cm^{-1}$ and $\Delta = 8.1(3)\ cm^{-1}$ for **4CuDy**, $J = 1.2(1)\ cm^{-1}$ and $\Delta = 7.4(2)\ cm^{-1}$ for **5CuEr**, and $J = -3.17(7)\ cm^{-1}$ and $\Delta = -18.2(2)\ cm^{-1}$ for **6CuYb** (Figure 5, bottom).

Due to the diamagnetism of the Ni^{II} cation, because of its square-planar geometry, from the magnetic point of view, the Ni^{II}–Ln^{III} (**6**–**12**) complexes should be assumed as mononuclear lanthanide compounds. $\chi_M T$ values for complexes **7NiCe**, **8NiGd**, **9NiTb**, **10NiDy**, **11NiEr**, and **12NiYb** are very close to the corresponding spin-only values for the isolated lanthanide cations $^2F_{5/2}$ (Ce^{III}, 0.80 $cm^3\ mol^{-1}\ K$), $^2S_{7/2}$ (Gd^{III}, 7.80 $cm^3\ mol^{-1}\ K$), $^7F_6$ (Tb^{III}, 11.84 $cm^3\ mol^{-1}\ K$), $^6H_{15/2}$ (Dy^{III}, 13.94 $cm^3\ mol^{-1}\ K$), $^4I_{15/2}$ (Er^{III}, 11.33 $cm^3\ mol^{-1}\ K$), $^2F_{7/2}$ ($2Yb^{III}$, 5.06 $cm^3\ mol^{-1}\ K$), respectively (Figure 5, top). The isotropic **8NiGd** complex shows the expected Curie response whereas the $\chi_M T$ values for the remaining compounds slowly decrease when lowering temperature due to the progressive depopulation of the Stark levels.

Dynamic Measurements. To study the dynamic magnetic properties, temperature and frequency variable alternate current (ac) measurements were performed on polycrystalline and pressed samples. No maxima appear in the out-of-phase measurements above 2 K for all complexes indicating that the magnetic moments completely follow the magnetic field due to the fast reversal of magnetization through quantum tunneling of the magnetization (QTM) between the low-lying ground state doublets. To try to suppress the QTM the samples were measured at 1000 Hz under different dc fields to explore their response (Figures S12 and S13).

For the {CuLn} family, these measurements revealed well defined $\chi_M''(T)$ peaks only for **2CuGd** and **3CuTb** (Figure 6), while for the {NiLn} family **7NiCe**, **8NiGd**, **10NiDy**, and **11NiEr** slowly relax under dc field (Figure 7). For **12NiYb**, only very weak tails were observed with increasing fields. $\chi_M'(T)$ plots are shown in Figures S14–S16. At this point, different approaches that require different treatments of the data were used for the calculation of the relaxation parameters of these systems.

Interestingly, the two gadolinium complexes **2CuGd** and **8NiGd**, based on a half-filled f^7 cation without orbital component and thus, with an expected isotropic response, exhibit clear out-of-phase peaks in their $\chi_M''(T)$ and $\chi_M''(\nu)$

https://doi.org/10.1021/acs.cgd.4c00598
Cryst. Growth Des. 2024, 24, 5806–5817

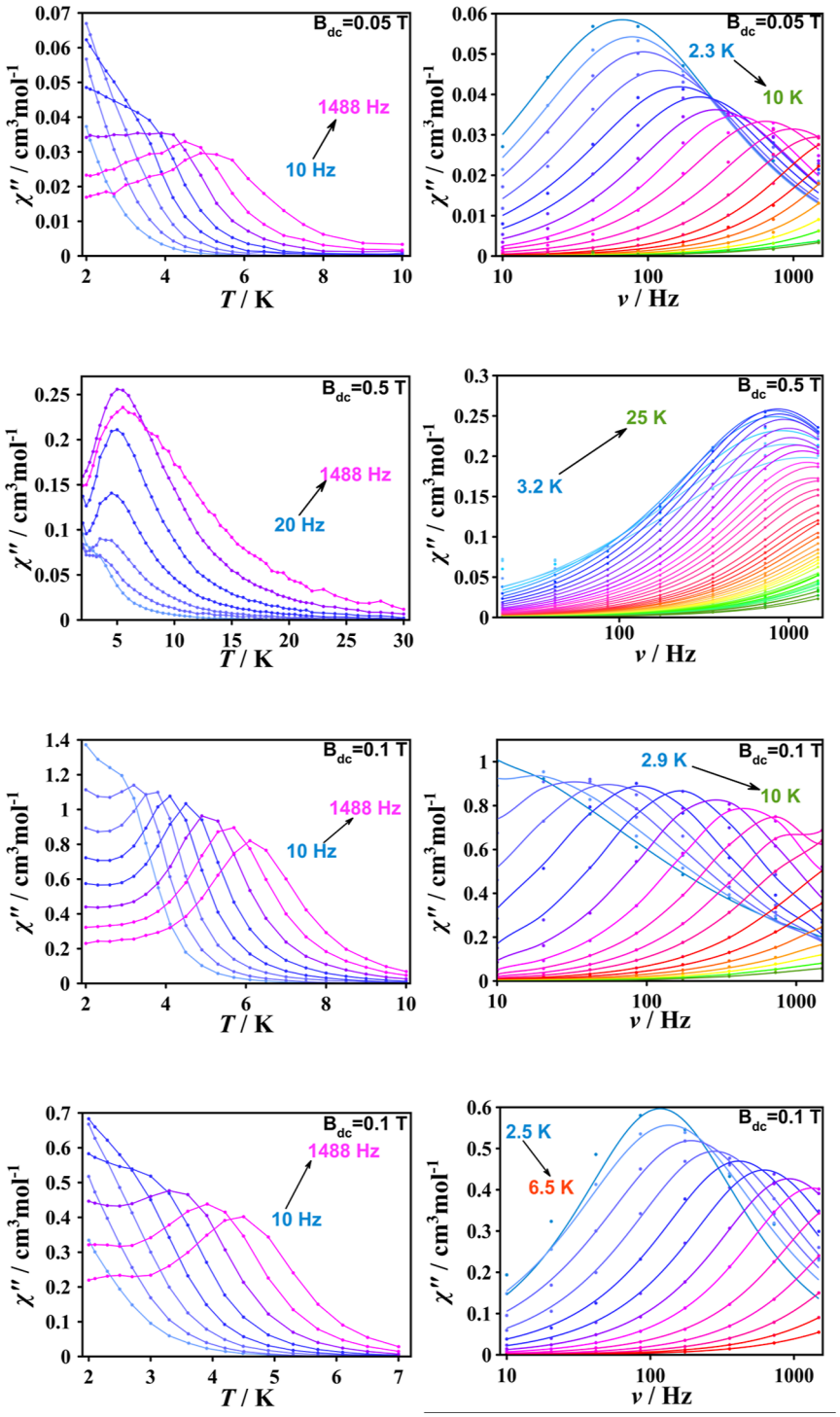

Figure 7. From top to bottom, temperature (left) and frequency (right) dependence of χ'' for complexes **7NiCe**, **8NiGd**, **10NiDy**, and **11NiEr**.

plots (Figures 6 and 7). The D value derived from the geometric distortions around the Gd^{III} cation is always low (0.1 cm^{-1} or lower) and then the usual barrier for the reversal of the magnetization, based on the value of the square of the S ground state and the D value, is negligible and the overbarrier Orbach relaxation mechanism is not operative in this case. Cole−Cole[45] plots (Figure 8) were fitted using CCfit software[46] and the generalized Debye model[47]

$$\chi(\omega) = \chi_S + (\chi_T + \chi_S)/(1 + i\omega\tau)^{1\alpha} \quad (3)$$

where χ_S and χ_T are the adiabatic and thermal susceptibilities respectively, τ is the average relaxation time, and α is a parameter ranging from 0 to 1 that defines the broadness of the spectra involving the distribution in the relaxation times. The relaxation times were analyzed excluding the Arrhenius-like behavior by means of the expression

$$\tau^{-1} = {\tau_{QTM}}^{-1} + AT + CT^n \quad (4)$$

in which the three terms take into account the QTM (${\tau_{QTM}}^{-1}$), Raman (BT^n), and direct (AT) processes, being n the Raman

https://doi.org/10.1021/acs.cgd.4c00598
Cryst. Growth Des. 2024, 24, 5806−5817

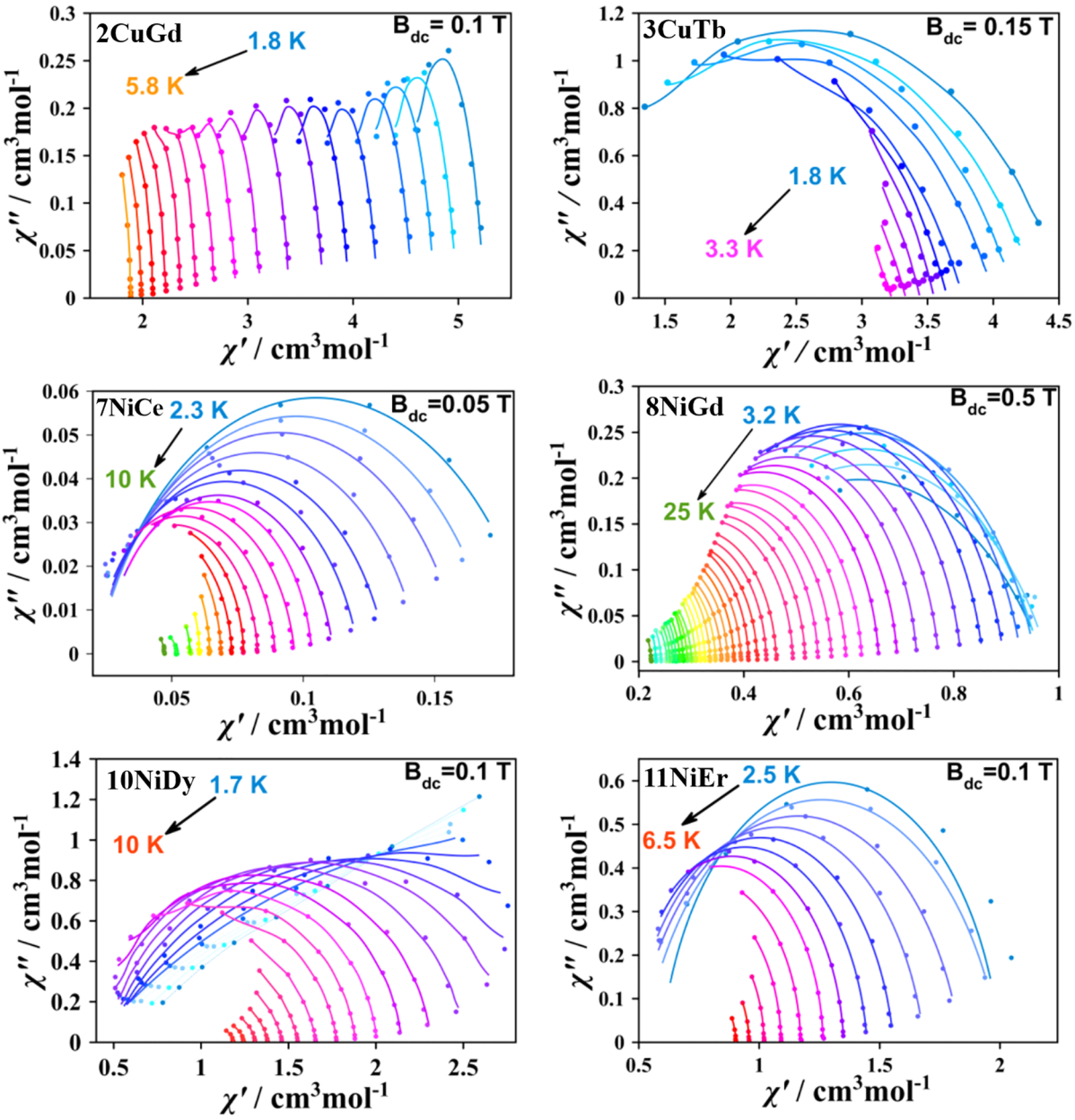

Figure 8. χ' vs χ'' representation. Experimental data are represented with dots and the fitting with solid line (dashed lines represent the temperatures without fitting).

coefficient, Figure 9, with the best fit parameters summarized in Table 3. The two complexes relax following direct plus Raman processes with a weak QTM contribution for **8NiGd** in agreement with Gd^{III} previously analyzed systems.[18−20,48]

For the remaining complexes, a well-defined ac response was found for **3CuTb** (Figure 6), **7NiCe**, **10NiDy**, and **11NiEr** (Figure 7) and tails of the peaks for **12NiYb** which will be analyzed separately. Ce^{III} belongs to the so-called uncommon lanthanides that in spite of its good SRM response and absence of nuclear spin have been poorly studied. Noteworthy, **7NiCe** is a new compound joining this family in Ce^{III} derived compounds exhibiting field-induced SRM.[49−52]

From the corresponding Cole−Cole plots of complexes **3CuTb**, **7NiCe**, **10NiDy**, and **11NiEr** (Figure 8), the relaxation rates were extracted and plotted as $\ln(\tau)$ in front of the inverse of the temperature in the so-called Arrhenius plots (Figure 9). The fit of the data was performed using eq 2

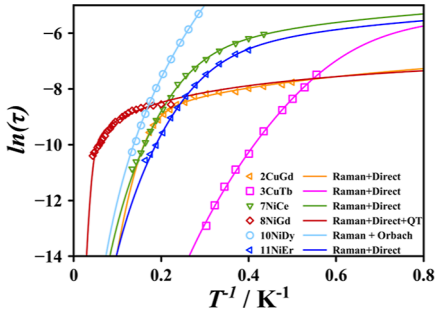

Figure 9. Plot ln (τ) vs $1/T$ for compounds **2CuGd**, **3CuTb**, **7NiCe**, **8NiGd**, **10NiDy**, and **11NiEr**. The solid line represents the best fitting relaxation processes.

including now the Arrhenius-like relaxation path, resulting in the expression

https://doi.org/10.1021/acs.cgd.4c00598
Cryst. Growth Des. 2024, 24, 5806−5817

Table 3. Best Fitting Relaxation Parameters for 2CuGd, 3CuTb, 7NiCe, 8NiGd, 10NiDy, 11NiEr, and 12NiYb

	C (s^{-1} K^{-n})	n	A (s^{-1} K^{-1})	τ_{QTM}^{-1}	U_{eff} (K)	τ_0 (s)
2CuGd	1.4(3)e-3	8.8(9)	1150(21)			
3CuTb	7.5(3)	9.0(5)	204(1)			
7NiCe	0.35(8)	6.0(1)	160(7)			
8NiGd		9.0(5)	879(22)	451		
10NiDy	5.7(6)e-4	8.99(7)			15.6(7)	1.2642×10^{-5}
11NiEr	0.7(1)	6.2(1)	203(13)			
12NiYb					4.23	8.23×10^{-5}

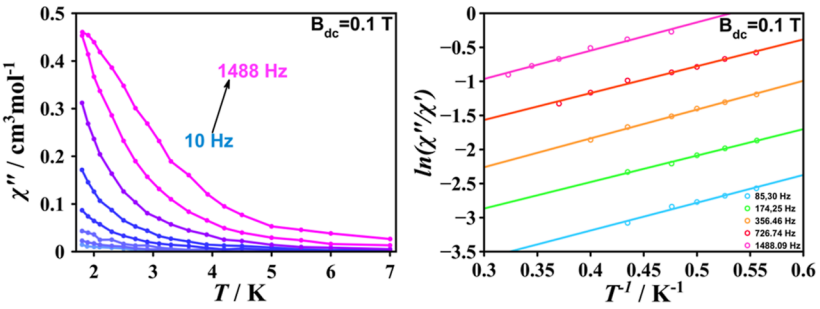

Figure 10. Left, temperature dependence of χ_M'' for **12NiYb** showing only weak tails. Right, fit of the data to obtain the apparent energy barrier.

$$\tau^{-1} = \tau_{QTM}^{-1} + AT + CT^n + \tau_0^{-1}\exp(-U_{eff}/K_BT) \quad (5)$$

Best fit values for **3CuTb**, **7NiCe**, **10NiDy**, and **11NiEr** are indicated in Table 3. **3CuTb**, **7NiCe**, and **11NiEr** show relaxation following direct plus Raman processes whereas the relaxation for **10NiDy** was best defined by Raman plus Arrhenius processes.

Due to the lack of information about the energy of the excited states that should be placed much higher than 15.6 cm^{-1}, we can only describe an Arrhenius-like behavior, without assigning an Orbach relaxation to the process for the high-temperature region in complex **10NiDy** and only reliable values for an apparent relaxation rate and effective energy barrier can be provided. The competition between more than one relaxation process for the six complexes can be evidenced in the representation of $\log(\tau)$ vs $\log(T)$ plots (Figures S17, S18) where two clearly different slopes in the curves indicate competition in between more than one relaxation pathway (Table S15). It is needed to mention that the controversial Raman coefficient lies in all cases in the expected range for a Kramers and for non-Kramers ion.

The case of complex **12NiYb** should be analyzed in a different way because, as has been said above, no maxima appeared in the $\chi_M''(T)$ curves and, thus, the Argand plots become too incomplete to extract reliable relaxation time values (Figure 10, left). This complex was analyzed using a previously reported method based on the generalized Debye model[47] which allows the calculation of an apparent energy barrier by representing the slope of the $\ln(\chi_M''/\chi_M')$ vs the inverse of the temperature (Figure 10, right). The calculated U_{eff} and τ_0 parameters for **12NiYb** are reported in Table 3.

Comparison with Previously Reported Systems. Despite that there are a wide number 3d/4f heterometallic dimers with bis-bidentate compartmental Schiff bases derived from *o*-vanillin, closely related with H_4L, Chart 2, most of the investigated properties are related to their luminescence (often ZnLn cores), dc magnetic properties (often on the CuGd system), or catalytic activity. In contrast, there are scarce studies about their ac response and focused on CuGd, CuDy, or CuTb systems. However, some interesting tendencies become remarkable for this family of comparable complexes.

Chart 2. Previously Reported Compartmental Ligands Related with H_4L

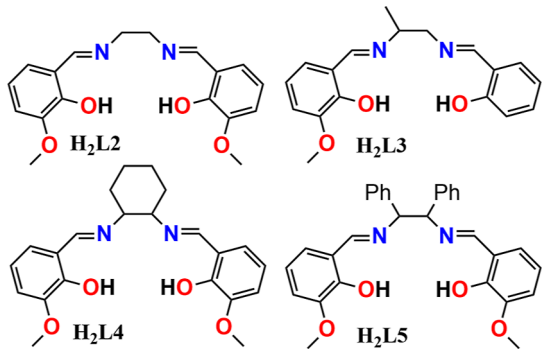

Slow relaxation of the magnetization for half-filled shell cations such Gd^{III}, which do not possess orbital contribution and thus are isotropic, has claimed the attention of magnetochemists over the recent years. Interestingly, all the studied cases with this kind of ligands and Gd^{III} with formula $[CuGdL3(NO_3)_3]$,[19] $[NiGdL5(NO_3)_3]$,[20] $[NiGdL2(Cl)_3(H_2O)]$[48] and complexes **2CuGd** and **8NiGd** exhibit this property, becoming the largest family of Gd^{III} systems with non-Orbach relaxation mechanism.

For the remaining cations, the only comparable complete series is the $[NiLnL5(NO_3)_3]$,[18] Ln^{III} = Ce, Nd, Dy, Er, and Yb in which all complexes exhibit slow relaxation of the magnetization as occurs with the reported $[LnNi(H_2L)(NO_3)_3]$ complexes **7NiCe**, **10NiDy**, **11NiEr**, and **12NiYb**. In addition to these two series, only four complexes with an equivalent formula, $[NiLnL4(NO_3)_3]$,[53] Ln^{III} = Dy and Tb and $[NiLnL2(Cl)_3(H_2O)]$[48] and Ln^{III} = Ce and Dy, have been reported, showing SRM in all cases.

The data are more limited for the CuLn system and more heterogeneous because there are anion variations. The only studied systems are $[CuDyL4(CH_3COO)_3]$,[54] $[CuTbL4(hfacac)_3]$,[55] $[CuLnL4(hfacac)_3]$[55] Ln^{III} = Tb, Dy, and Ho

https://doi.org/10.1021/acs.cgd.4c00598
Cryst. Growth Des. 2024, 24, 5806−5817

and **3CuTb** which also show SRM. However, despite the limited data what becomes interesting is the feature of the better response of the NiLn systems in comparison with the CuLn-related complexes for which ac response has been not found for [CuLnL3$(NO_3)_3$],[56] Ln^{III} = Tb and Dy as well as **1CuCe**, **4CuDy**, **5CuEr**, and **6CuYb**.

CONCLUSIONS

The compartmental H_4L Schiff base obtained by condensation of ethylenediamine and 2,3-dihydroxybenzaldehyde proved to be useful to generate heterometallic 3*d*/4f structures in their deprotonate H_2L^{2-} and HL^{3-} forms. The two series of {CuLn} and {NiLn} complexes (Ln = Ce, Gd, Tb, Dy, Er, Yb) have been structurally characterized. The **2CuGd** and **8NiGd** complexes derived from the isotropic Gd^{III} cation exhibit a field-induced slow relaxation of the magnetization, following the relaxation Raman plus direct processes. For the members of the series with orbital momentum $L \neq 0$ slow relaxation of the magnetization was found for **3CuTb**, **7NiCe**, **10NiDy**, **11NiEr**, and **12NiYb**. From our data and the comparison with reported related systems, it can be realized that coupled Cu^{II}–Ln^{III} systems rarely exhibit slow relaxation of the magnetization in contrast with the Ni^{II}–Ln^{III} complexes in which the square planar Ni^{II} cation is diamagnetic.

ASSOCIATED CONTENT

Supporting Information

The Supporting Information is available free of charge at https://pubs.acs.org/doi/10.1021/acs.cgd.4c00598.

Characterization, crystallographic, and complementary magnetic information (PDF)

Accession Codes

CCDC 2286750–2286755 and 2313343 contain the supplementary crystallographic data for this paper. These data can be obtained free of charge via www.ccdc.cam.ac.uk/data_request/cif, or by emailing data_request@ccdc.cam.ac.uk, or by contacting The Cambridge Crystallographic Data Centre, 12 Union Road, Cambridge CB2 1EZ, UK; fax: +44 1223 336033.

AUTHOR INFORMATION

Corresponding Author

Albert Escuer − *Departament de Química Inorgànica i Orgànica, secció Inorgànica, Universitat de Barcelona, Barcelona 08028, Spain; Institut de Nanociència i Nanotecnologia (IN2UB), Universitat de Barcelona, Barcelona 08028, Spain;* orcid.org/0000-0002-6274-6866; Email: albert.escuer@qi.ub.edu

Authors

Ernesto Costa-Villén − *Departament de Química Inorgànica i Orgànica, secció Inorgànica, Universitat de Barcelona, Barcelona 08028, Spain*

Mercè Font-Bardia − *Departament de Mineralogia, Cristal·lografia i Dipòsits Minerals and Unitat de Difracció de R-X, Centre Científic i Tecnològic de la Universitat de Barcelona (CCiT-UB), Universitat de Barcelona, Barcelona 08028, Spain*

Júlia Mayans − *Departament de Química Inorgànica i Orgànica, secció Inorgànica, Universitat de Barcelona, Barcelona 08028, Spain; Institut de Nanociència i Nanotecnologia (IN2UB), Universitat de Barcelona, Barcelona 08028, Spain;* orcid.org/0000-0001-8875-8075

Complete contact information is available at: https://pubs.acs.org/10.1021/acs.cgd.4c00598

Author Contributions

The manuscript was written through contributions of all authors. All authors have given approval to the final version of the manuscript.

Notes

The authors declare no competing financial interest.

REFERENCES

(1) Adam, M. S. S.; El-Hady, O. M.; Ullah, F. Biological and catalytic potential of sustainable low and high valent metal-Schiff base sulfonate salicylidene pincer complexes. *RSC Adv.* **2019**, *9*, 34311–34329.

(2) Nath, M.; Saini, P. K. Chemistry and applications of organotin(iv) complexes of Schiff bases. *Dalton Trans.* **2011**, *40*, 7077–7121.

(3) Hou, X. X.; Ren, Y. P.; Luo, Z. H.; Jiang, B. L.; Lu, T. T.; Huang, F. P.; Qin, X. Y. Two novel chiral tetranucleate copper-based complexes: syntheses, crystal structures, inhibition of angiogenesis and the growth of human breast cancer in vitro and in vivo. *Dalton Trans.* **2021**, *50*, 14684–14694.

(4) Singh, D. P.; Allam, B. K.; Singh, K. N.; Singh, V. P. A binuclear Mn(II) complex as an efficient catalyst for transamidation of carboxamides with amines. *RSC Adv.* **2014**, *4*, 1155–1158.

(5) Karvembu, R.; Hemalatha, S.; Prabhakaran, R.; Natarajan, K. Synthesis, characterization and catalytic activities of ruthenium complexes containing triphenylphosphine/triphenylarsine and tetradentate Schiff bases. *Inorg. Chem. Commun.* **2003**, *6*, 486–490.

(6) Kaur, M.; Kumar, S.; Yusuf, M.; Lee, J.; Brown, R. J. C.; Kim, K. H.; Malik, A. K. Post-synthetic modification of luminescent metal-organic frameworks using schiff base complexes for biological and chemical sensing. *Coord. Chem. Rev.* **2021**, *449*, 214214.

(7) Berhanu, A. L.; Gaurav; Mohiuddin, I.; Malik, A. K.; Aulakh, J. S.; Kumar, V.; Kim, K. H. A review of the applications of Schiff bases as optical chemical sensors. *TrAC, Trends Anal. Chem.* **2019**, *116*, 74–91.

(8) Archer, R. D.; Chen, H.; Thompson, L. C. Synthesis, Characterization, and Luminescence of Europium(III) Schiff Base Complexes[1a]. *Inorg. Chem.* **1998**, *37*, 2089–2095.

(9) Riddle, J. A.; Lathrop, S. P.; Bollinger, J. C.; Lee, D. Schiff base route to stackable pseudo-triphenylenes: stereoelectronic control of assembly and luminescence. *J. Am. Chem. Soc.* **2006**, *128*, 10986–10987.

(10) Pasatoiu, T. D.; Etienne, M.; Madalan, A. M.; Andruh, M.; Sessoli, R. Dimers and chains of {3d-4f} single molecule magnets constructed from heterobimetallic tectons. *Dalton Trans.* **2010**, *39*, 4802–4808.

(11) Andruh, M. The exceptionally rich coordination chemistry generated by Schiff base ligands derived from o-vanillin. *Dalton Trans.* **2015**, *44*, 16633–16653.

(12) Kaczmarek, M. T.; Zabiszak, M.; Nowak, M.; Jastrzab, R. Lanthanides: Schiff base complexes, applications in cancer diagnosis, therapy, and antibacterial activity. *Coord. Chem. Rev.* **2018**, *370*, 42–54.

(13) Shi, L.; Ge, H. M.; Tan, S. H.; Li, H. Q.; Song, Y. C.; Zhu, H. L.; Tan, R. X. Synthesis and antimicrobial activities of Schiff bases derived from 5-chloro-salicylaldehyde. *Eur. J. Med. Chem.* **2007**, *42*, 558–564.

(14) Hahn, P.; Ullmann, S.; Klose, J.; Peng, Y.; Powell, A. K.; Kersting, B. Dinuclear Tb and Dy complexes supported by hybrid Schiff-base/calixarene ligands: synthesis, structures and magnetic properties. *Dalton Trans.* **2020**, *49*, 10901–10908.

(15) Alexopoulou, K. I.; Terzis, A.; Raptopoulou, C. P.; Psycharis, V.; Escuer, A.; Perlepes, S. P. Ni^{II}_{20} "Bowls" from the Use of Tridentate Schiff Bases. *Inorg. Chem.* **2015**, *54*, 5615−5617.
(16) Costes, J. P.; Duhayon, C.; Vendier, L.; Mota, A. J. Reaction of a series of ZnL, CuL and NiL Schiff base and non-Schiff base complexes with MCl_2 salts (M = Cu, Ni, Mn). Syntheses, structures, magnetic properties and DFT calculations. *New J. Chem.* **2018**, *42*, 3683−3691.
(17) Mayans, J.; Font-Bardia, M.; Escuer, A. Chiroptical and magnetic properties of star-shaped Fe^{III}_4 complexes from chiral Schiff bases. Structural and magnetic correlations based on continuous shape measures. *Dalton Trans.* **2018**, *47*, 8392−8401.
(18) Mayans, J.; Saez, Q.; Font-Bardia, M.; Escuer, A. Enhancement of magnetic relaxation properties with 3d diamagnetic cations in $[Zn^{II}Ln^{III}]$ and $[Ni^{II}Ln^{III}]$, Ln^{III} = Kramers lanthanides. *Dalton Trans.* **2019**, *48*, 641−652.
(19) Ghosh, T. K.; Maity, S.; Mayans, J.; Ghosh, A. Family of Isomeric Cu^{II}-Ln^{III} (Ln = Gd, Tb, and Dy) complexes presenting field-induced slow relaxation of magnetization only for the members containing Gd^{III}. *Inorg. Chem.* **2021**, *60*, 438−448.
(20) Mayans, J.; Escuer, A. Correlating the axial zero field splitting with the slow magnetic relaxation in Gd^{III} SIMs. *Chem. Commun.* **2021**, *57*, 721−724.
(21) Pilichos, E.; Font-Bardia, M.; Escuer, A.; Mayans, J. Structural and magnetic studies of mononuclear lanthanide complexes derived from N-rich chiral Schiff bases. *Dalton Trans.* **2021**, *50*, 1746−1753.
(22) Bhunia, P.; Maity, S.; Mayans, J.; Ghosh, A. Templated synthesis of Ni(II) complexes of unsymmetrical Schiff base ligands derived from 1,3-diamino-2-propanol: structural diversity and magnetic properties. *New J. Chem.* **2022**, *46*, 4363−4372.
(23) Caballero, S.; Pilichos, E.; Font-Bardia, M.; Mayans, J.; Escuer, A. Field-induced slow magnetic relaxation in a new family of Tetranuclear Double-Stranded Cu_2^{II}-Ln_2^{III} metallohelicates. *Cryst. Growth Des.* **2023**, *23*, 3711−3719.
(24) Salmon, L.; Thuery, P.; Ephritikhine, M. Polynuclear uranium(IV) compounds with (μ_3-oxo)U_3 or (μ_4-oxo)U_4 cores and compartmental Schiff base ligands. *Polyhedron* **2006**, *25*, 1537−1542.
(25) Salmon, L.; Thuery, P.; Riviere, E.; Girerd, J. J.; Ephritikhine, M. Structure and magnetism of the first strictly dinuclear compound containing paramagnetic 3d and 5f metal ions. Major influence of the Cu^{II} ion coordination on the exchange Cu^{II}-U^{IV} interaction. *Chem. Commun.* **2003**, 762−763.
(26) Salmon, L.; Thuery, P.; Ephritikhine, M. Crystal structure of hetero(bi- and tetra-)metallic complexes of compartmental Schiff bases uniting uranyl and transition metal (Ni^{2+}, Cu^{2+}) ions. *Polyhedron* **2003**, *22*, 2683−2688.
(27) Salmon, L.; Thuery, P.; Ephritikhine, M. A bis-(acetylacetonato)-uranium(IV) complex of the Schiff base N,N′-bis(3-hydroxy-salicyl-idene)-2-methyl-1,2-propane-di-amine. *Acta Crystallogr., Sect. C: Cryst. Struct. Commun.* **2003**, *59*, m246−m248.
(28) Salmon, L.; Thuery, P.; Riviere, E.; Ephritikhine, M. Synthesis, structure, and magnetic behavior of a series of trinuclear Schiff base complexes of 5f (U^{IV}, Th^{IV}) and 3d (Cu^{II}, Zn^{II}) ions. *Inorg. Chem.* **2006**, *45*, 83−93.
(29) Cametti, M.; Ilander, L.; Rissanen, K. Recognition of Li^+ by a salophen-UO_2 homodimeric complex. *Inorg. Chem.* **2009**, *48*, 8632−8637.
(30) Salmon, L.; Thuery, P.; Ephritikhine, M. Synthesis and crystal structure of tetra- and hexanuclear uranium(iv) complexes with hexadentate compartmental Schiff-base ligands. *Dalton Trans.* **2004**, 4139−4145.
(31) Salmon, L.; Thuery, P.; Ephritikhine, M. Strictly hetero-dinuclear compounds containing U^{4+} and Cu^{2+} or Ni^{2+} ions. *Polyhedron* **2007**, *26*, 645−652.
(32) Salmon, L.; Thuery, P.; Riviere, E.; Girerd, J. J.; Ephritikhine, M. Versatility of the nature of the magnetic Cu(II)-U(IV) interaction. Syntheses, crystal structures and magnetic properties of Cu_2U and CuU compounds. *Dalton Trans.* **2003**, 2872−2880.
(33) Hill, R. J.; Rickard, C. E. F. Complexes of thorium(IV) and uranium(IV) with some Schiff bases. *J. Inorg. Nucl. Chem.* **1978**, *40*, 793−797.
(34) Cheira, M. F.; Orabi, A. S.; Atia, B. M.; Hassan, S. M. Solvent extraction and separation of Thorium(IV) from chloride media by a Schiff base. *J. Solution Chem.* **2018**, *47*, 611−633.
(35) Hu, K. Q.; Wu, S. Q.; Cui, A. L.; Kou, H. Z. Synthesis, structure, and magnetic properties of heterotrimetallic tetranuclear complexes. *Transition Met. Chem.* **2014**, *39*, 713−718.
(36) Sheldrick, G. M. SHELXL-2014/7: Program for the Solution of Crystal Structures; University of Göttingen: Göttingen, Germany, 2014.
(37) Bain, G. A.; Berry, J. F. Diamagnetic corrections and Pascal's constants. *J. Chem. Educ.* **2008**, *85*, 532−536.
(38) Aguiari, A.; Bullita, E.; Casellato, U.; Guerriero, P.; Tamburini, S.; Vigato, P. A. Macrocyclic and macroacyclic compartmental Schiff bases: synthesis, characterization, X-ray structure and interaction with metal ions. *Inorg. Chim. Acta* **1992**, *202*, 157−171.
(39) Lunell, M.; Casanova, D.; Cirera, J.; Alemany, P.; Alvarez, S. *SHAPE* v.2.0.; Barcelona, 2010. The program can be obtained by request to the authors.
(40) Chilton, N. F.; Anderson, R. P.; Turner, L. D.; Soncini, A.; Murray, K. S. PHI: A powerful new program for the analysis of anisotropic monomeric and exchange-coupled polynuclear *d*- and *f*-block complexes. *J. Comput. Chem.* **2013**, *34*, 1164−1175.
(41) Novitchi, G.; Shova, S.; Caneschi, A.; Costes, J. P.; Gdaniec, M.; Stanica, N. Hetero di- and trinuclear Cu-Gd complexes with trifluoroacetate bridges: synthesis, structural and magnetic studies. *Dalton Trans.* **2004**, 1194−1200.
(42) Fellah, F. Z. C.; Costes, J. P.; Dahan, F.; Duhayon, C.; Novitchi, G.; Tuchagues, J. P.; Vendier, L. Di- and triheteronuclear Cu-Gd and Cu-Gd-Cu complexes with dissymmetric double bridge. *Inorg. Chem.* **2008**, *47*, 6444−6451.
(43) Cremades, E.; Gómez-Coca, S.; Aravena, D.; Alvarez, S.; Ruiz, E. Theoretical study of exchange coupling in 3d-Gd complexes: large magnetocaloric effect systems. *J. Am. Chem. Soc.* **2012**, *134*, 10532−10542.
(44) Rajaraman, G.; Totti, F.; Bencini, A.; Caneschi, A.; Sessoli, R.; Gatteschi, D. Density functional studies on the exchange interaction of a dinuclear Gd(III)-Cu(II) complex: method assessment, magnetic coupling mechanism and magneto-structural correlations. *Dalton Trans.* **2009**, 3153−3161.
(45) Cole, K. S.; Cole, R. H. J. Dispersion and absorption in dielectrics I. Alternating current characteristics. *Chem. Phys.* **1941**, *9*, 341−351.
(46) Reta, D.; Chilton, N. F. Uncertainty estimates for magnetic relaxation times and magnetic relaxation parameters. *Phys. Chem. Chem. Phys.* **2019**, *21*, 23567−23575.
(47) Debye, P. The paramagnetic relaxation. *Phys. Z.* **1938**, *39*, 616−618.
(48) Vráblová, A.; Tomás, M.; Falvello, L. R.; Dlháň, L'.; Titiš, J.; Černák, J.; Boča, R. Slow magnetic relaxation in Ni-Ln (Ln = Ce, Gd, Dy) dinuclear complexes. *Dalton Trans.* **2019**, *48*, 13943−13952.
(49) Hino, S.; Maeda, M.; Yamashita, K.; Kataoka, Y.; Nakano, M.; Yamamura, T.; Nojiri, H.; Kofu, M.; Yamamuro, O.; Kajiwara, T. Linear trinuclear Zn(II)-Ce(III)-Zn(II) complex which behaves as a single-molecule magnet. *Dalton Trans.* **2013**, *42*, 2683−2686.
(50) Mayans, J.; Tesi, L.; Briganti, M.; Boulon, M. E.; Font-Bardia, M.; Escuer, A.; Sorace, L. Single ion anisotropy and intramolecular interactions in Ce^{III} and Nd^{III} dimers. *Inorg. Chem.* **2021**, *60*, 8692−8703.
(51) Tubau, A.; Gómez-Coca, S.; Speed, S.; Font-Bardía, M.; Vicente, R. New series of mononuclear β-diketonate cerium(iii) field induced single-molecule magnets. *Dalton Trans.* **2024**, *53*, 9387−9405.
(52) Singh, S. K.; Gupta, T.; Ungur, L.; Rajaraman, G. Magnetic Relaxation in Single-Electron Single-Ion Cerium (III) Magnets: Insights from Ab Initio Calculations. *Chem.—Eur. J.* **2015**, *21*, 13812−13819.

https://doi.org/10.1021/acs.cgd.4c00598
Cryst. Growth Des. 2024, 24, 5806−5817

(53) Wen, H. R.; Liu, S. J.; Xie, X. R.; Bao, J.; Liu, C. M.; Chen, J. L. A family of nickel-lanthanide heterometallic dinuclear complexes derived from a chiral Schiff-base ligand exhibiting single-molecule magnet behaviors. *Inorg. Chim. Acta* **2015**, *435*, 274−282.
(54) Zhang, P.; Zhang, L.; Lin, S. Y.; Tang, J. Tetranuclear $[MDy]_2$ compounds and their dinuclear [MDy] (M = Zn/Cu) building units: their assembly, structures, and magnetic properties. *Inorg. Chem.* **2013**, *52*, 6595−6602.
(55) Wang, K.; Zhang, J.; Lu, J.; Jing, P.; Li, L. Slow magnetic relaxation in Cu-Ln heterometallic Schiff base complexes containing $Ln(hfac)^{4-}$ as counterions. *Inorg. Chim. Acta* **2019**, *490*, 51−56.
(56) Wen, H. R.; Bao, J.; Liu, S. J.; Liu, C. M.; Zhang, C. W.; Tang, Y. Z. Temperature-controlled polymorphism of chiral CuII-LnIII dinuclear complexes exhibiting slow magnetic relaxation. *Dalton Trans.* **2015**, *44*, 11191−11201.

https://doi.org/10.1021/acs.cgd.4c00598
Cryst. Growth Des. 2024, 24, 5806−5817